Sedimentation process of saturated sand under impact loading

ZHANG Junfeng & MENG Xiangyue

Institute of Mechanics, Chinese Academy of Sciences, Beijing 100080, China
Correspondence should be addressed to Zhang Junfeng (email: zhangjf@imech.ac.cn)
Received July 1, 2004; accepted November 9, 2004

Abstract The initial small inhomogeneity of saturated sand could be amplified during the sedimentation process after liquefaction, and cracks could be observed in the sand column. Layers of fine sand could also be found at the exact place where cracks developed and disappeared. The phenomena and the whole process were experimentally shown by X-rays images. To account for the phenomena, a linearized stability analysis of the sedimentation of saturated sand was conducted; however, it did not produce a satisfactory result. A three-phase flow model describing the transportation of fine sand is presented in this paper. It is shown that such a kind of erosion/deposition model was qualitatively in good agreement with the experimental observation.

Keywords: sedimentation process, liquefaction, stability analysis, three-phase flow model.

DOI: 10.1360/04zze6

1 Introduction

Experimental studies on the formation of horizontal cracks in vertical columns of saturated sand contained in circular cylinders have been reported in two recent papers[1,2]. In ref. [1] the cylinder was subjected to an axial impact. In ref. [2] a steady flow of water was driven upward through the sand column sitting on a perforated rigid diaphragm. In both cases, care was taken in preparing the sand sample by feeding wetted uniform sand continuously into a column to avoid intentional stratification. However, a small degree of inhomogeneity still existed.

Although the detailed description on experimental phenomena in sedimentation and drainage process was presented in refs. [1,2], the horizontal cracks could only be seen outside of a sand column and small drainage outlets could be observed at the upper surface of the sand column. Further experiments showed that the size distribution of sand grains was important. The cracks appeared only when the range of the size distribution of sand grains was broad, especially when fine sand played a important role in the formation of cracks.

It seems that the boundary effect is the main cause for cracks developing in saturated sand and no drainage pathway exists for pore water flowing upward.

To show if cracks can develop throughout the whole cross-section where they are observed from outside and drainage pathways do exist not only at the upper surface of sand but also throughout the depth of the sand skeleton, an X-ray machine was used to get the image of the sedimentation process of saturated sand. It showed that the inhomogeneity of a sand sample plays a significant role for the formation of cracks, and some longitudinal drainage pathways can develop during the closing of horizontal cracks.

In the literature, the concept of "water film" was first suggested by Seed[3] in attempting to explain slope failure observed in earthquakes. Such a slope failure was developed in a sand bed containing an impermeable layer. Fiegal and Kutter[4] also demonstrated the formation of water films in layered sand in a centrifugal shake table test. Kobusho[5] performed shaking table tests using a sand sample containing a seam of non-plastic silt about 4 mm thick subjected to horizontal shocks to simulate earthquakes, and showed that a water film was formed underneath the silt layer. In the present paper we prefer to use "crack" to "water film" in order to give attention to the change of sand skeleton.

Both refs. [1] and [2] mentioned that liquefaction was a necessary condition for the initiation and development of cracks. In ref. [1], the cracks were initiated at about 20 s after liquefaction but impact loading only lasted several milliseconds. So it is natural to reason that the cracks are developed during the sedimentation process, and the stability of the sedimentation process should be analyzed first.

Prosperitti and Satrape[6] discussed the stability and hyperbolic properties of a very broad class of two-phase flow models that included many specific examples proposed in the earlier literature. In spite of the presence of non-differential "source" terms in the equations, their study showed that the stability of steady uniform flows was independent of the wave number of the perturbation. As a consequence, hyperbolicity was only necessary, but not sufficient, for stability. In the present paper, we also conduct a stability analysis of the sedimentation and percolation process for liquefied saturated sand, thereby trying to find the reason for the formation of cracks.

The stability analysis obviously cannot give the condition for the initiation of cracks. Cheng et al.[7] proposed a model to discuss the formation of horizontal cracks in a vertical column of saturated sand, in which they introduced the third phase, namely fine sand having the same velocity as the pore water. The three-phase flow model was thus used in this study to discuss the transportation of fine sand in general cases, but only the application of this kind of model in a specific case is presented. Theoretical result of the accumulation of fine sand in the transportation process can be verified using X-ray images.

2 Experimentation

To study the initiation and development of cracks, we used a video camera to record

the whole process from the lateral side. This method was proved to be effective[1]. The opening and closing of cracks could be observed clearly at any time, but this method could not be used in the study of the drainage pathways because the visible light could not penetrate the sand column. We also tried to use ultrasonic waves to detect the existence of drainage pathways, but our efforts failed because of the small size of pathways and strong chromatic dispersion of waves in saturated sand. The so-called X-ray method was adopted by Baxter et al.[8] to study the flow pattern of dry sand in a flat hopper.

Both a pulse X-ray machine and a clinical X-ray machine were used to compare the experimental result, since these two kinds of X-rays' wavelengths and penetration capabilities are different. Some characteristics of these two kinds of X-rays are given in Table 1.

Table 1 Comparison of Characteristics

Type	Wavelength/Å	Voltage/kV	Amperage	Duration time	Advantages and disadvantages
Pulse X-ray	0.006—0.6	0—450	10^4 A	20 ns	high density, thicker, but one image
Clinical X-ray	6—60	0—120	several mA	several ms	continuous images

In order to distinguish drainage pathways on images obtained by using pulse X-rays, some materials possessing larger atomic number elements such as $BaSO_4$, ZnO and TiO_2 were used as tracing materials. Each of their densities is about twice as much as that of the saturated sand sample (1.9×10^3 kg/m^3). The tracing materials could be shown clearly in X-ray films, but no drainage pathway could be distinguished. When the upper surface of the sand sample was inspected, we found that the main material carried by upward flowing water was fine sand. The averaging process of the image blurred the profile of the drainage pathways. Therefore, the pulse X-ray method is not suitable to study the flow of porous water in saturated sand. It is mainly used to detect damage in metal or in the case that the difference between densities of materials is large.

To show the effect of the clinical X-ray method, we installed some thin plastic pipes in a sand sample contained in a flat plexiglas box of 145 mm×33 mm×280 mm. The diameters of the plastic pipes range from 2 to 5 mm. Each plastic pipe was filled with water, coarse sand, fine sand, and dense or loose sand, separately. Experimental results proved that the plastic pipes could be seen clearly on the monitor. One of such images is shown in Fig. 1.

It is obvious that such a kind of method can be used to detect cracks and drainage pathways in saturated sand. Figs. 2—4 were taken using the same experimental procedure. Figs. 2 and 4 demonstrate respectively the states of a sand sample before liquefaction and after reconsolidation, while Fig. 3 shows the state of cracks in sand sample at one moment in the sedimentation process.

In Fig. 2, it is shown that the initial inhomogeneity still existed although the sand sample was filled continuously to avoid intentional stratification. In Fig. 3, some cracks

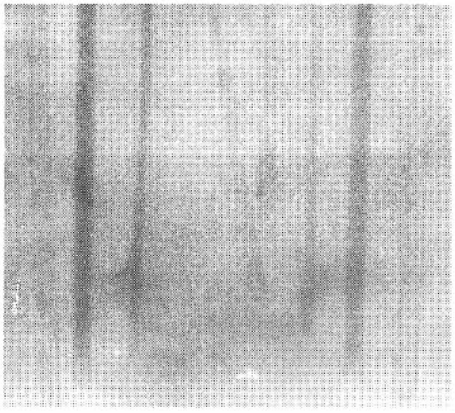

Fig.1. X-ray image of plastic pipes in saturated sand.

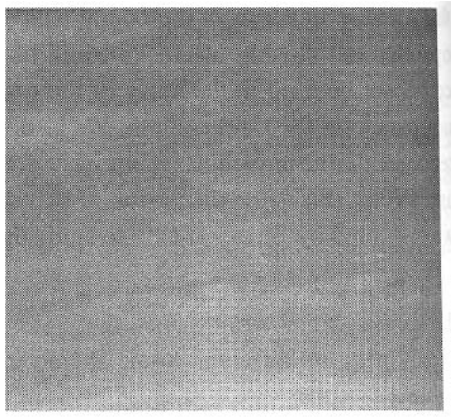

Fig. 2. X-ray image of initial sand sample.

were initiated just underneath fine sand layers, and drainage pathways might form at the ends of cracks. It could also be seen that horizontal stratification became concave upward because of sedimentation and boundary effect. Fig. 4 shows that the initial inhomogeneity was amplified and formed several layers of fine sand.

The experimental results showed that cracks and drainage pathways indeed existed in saturated sand during the sedimentation process. The initial inhomogeneity might be amplified and further developed into layers of fine sand because of transportation. Some drainage pathways were initiated at the end of cracks, and some near the boundary.

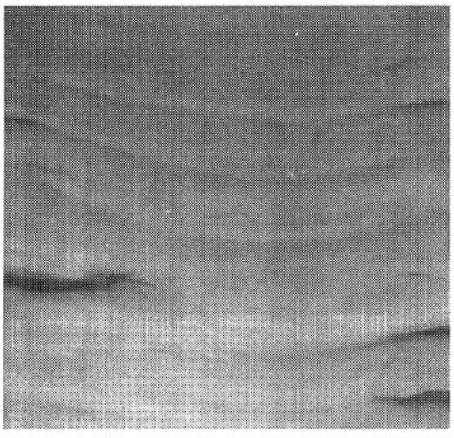

Fig. 3. X-ray image of cracks in saturated sand.

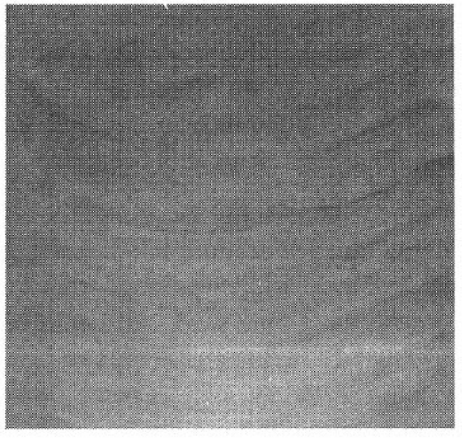

Fig. 4. X-ray image of sand sample after reconsolidation.

3 Linear stability analysis

In ref. [1], cracks appeared at about 20 s after the fluctuating process began, and in ref. [2], cracks also developed in the liquefied region of saturated sand. It is thus reasonable to speculate that cracks developed during the sedimentation process may have some relationship to the stability of the seepage of pore water.

In this study, we conducted stability analysis using a two-phase flow model. Considering the sedimentation of a mixture of sand particles and water contained in a vertical column, we assumed that the following properties were satisfied for the solid-fluid system: (i) The mixture of saturated sand is completely liquefied before the sedimentation begins and the sand skeleton loses any resistance; (ii) the sand particles are small with respect to the container and have the same density; (iii) the solid and fluid constituents of the liquefied sand are incompressible; (iv) there is no mass transfer between the solid and the fluid during sedimentation; (v) the void of liquefied sand in the same cross-section is equal.

Mass and momentum conservation laws can form the constitutive equations and the interactive term between fluid and solid obeys Darcy's law:

$$\frac{\partial \varepsilon}{\partial t}+\frac{\partial \varepsilon u}{\partial x}=0, \tag{1}$$

$$\frac{\partial (1-\varepsilon)\rho_s}{\partial t}+\frac{\partial (1-\varepsilon)\rho_s u_s}{\partial x}=0, \tag{2}$$

$$\varepsilon\rho\left(\frac{\partial u}{\partial t}+u\frac{\partial u}{\partial x}\right)+\varepsilon\frac{\partial p}{\partial x}+\varepsilon\rho g+F=0, \tag{3}$$

$$(1-\varepsilon)\rho_s\left(\frac{\partial u_s}{\partial t}+u_s\frac{\partial u_s}{\partial x}\right)+(1-\varepsilon)\frac{\partial p}{\partial x}+(1-\varepsilon)\rho_s g-F=0, \tag{4}$$

where t is time, and x is the coordinate pointing upward with an origin at the bottom of the sand column. ε is the porosity of the sand sample, u the velocity of the pore water, and u_s the velocity of sand grains. ρ and ρ_s are the densities of pore water and sand grains respectively. Both of them are constant according to assumption (3) above. g is the gravitational acceleration, and F is the interactive term. Given that F is related to the porosity and permeability of the sand sample, we assumed that it is expressed in the following form:

$$F=\frac{\mu(1-\varepsilon)\varepsilon^2}{K_0(1-\varepsilon_0)}(u-u_s), \tag{5}$$

where μ is the coefficient of viscosity, ε_0 and K_0 are the initial porosity and permeability of the sand sample respectively.

Eliminating $\frac{\partial p}{\partial x}$ in eqs.(3) and (4), eqs. (1)—(5) can be simplified as

$$\frac{\partial \varepsilon}{\partial t}+\frac{\partial \varepsilon u}{\partial x}=0, \tag{6}$$

$$\frac{\partial \varepsilon}{\partial t}-\frac{\partial(1-\varepsilon)u_s}{\partial x}=0, \tag{7}$$

$$\left(\frac{\partial u_s}{\partial t}+u_s\frac{\partial u_s}{\partial x}\right)-\frac{\rho}{\rho_s}\left(\frac{\partial u}{\partial t}+u\frac{\partial u}{\partial x}\right)+\left(1-\frac{\rho}{\rho_s}\right)g-\frac{\mu\varepsilon}{\rho_s k_0(1-\varepsilon_0)}(u-u_s)=0. \tag{8}$$

The basic constant solutions satisfying the problem are

$$\varepsilon=\varepsilon_0=\text{const}, \tag{9a}$$

$$u=u_0=\text{const}, \tag{9b}$$

$$u_s=u_{s0}=\text{const}, \tag{9c}$$

$$\frac{\partial p}{\partial x}=\frac{\partial p_0}{\partial x}=[\varepsilon_0\rho+(1-\varepsilon_0)\rho_s]g, \tag{9d}$$

$$F=F_0=\frac{\mu}{K_0}\varepsilon_0^2(u-u_s). \tag{9e}$$

Now we take ρ_s, g and $\dfrac{\mu}{K_0(1-\varepsilon_0)}$ as independent quantities, the dimensionless forms of other quantities in eqs. (6)—(8) are

$$\bar{t}=\frac{\mu}{\rho_s k_0(1-\varepsilon_0)}\cdot t, \qquad \bar{x}=\left(\frac{\mu}{\mu\rho_s k_0(1-\varepsilon_0)}\right)^2\cdot\frac{x}{g},$$

$$\bar{\rho}=\frac{\rho}{\rho_s}, \qquad \bar{u}=\frac{\mu}{\rho_s k_0(1-\varepsilon_0)g}\cdot u, \qquad \bar{u}_s=\frac{\mu}{\rho_s k_0(1-\varepsilon_0)g}\cdot u_s.$$

Transforming eqs. (6)—(8) into dimensionless form, we have

$$\frac{\partial \varepsilon}{\partial \bar{t}}+\frac{\partial \varepsilon\bar{u}}{\partial \bar{x}}=0, \tag{10a}$$

$$\frac{\partial \varepsilon}{\partial \bar{t}}-\frac{\partial(1-\varepsilon)\bar{u}_s}{\partial \bar{x}}=0, \tag{10b}$$

$$\left(\frac{\partial \bar{u}_s}{\partial \bar{t}}+\bar{u}_s\frac{\partial \bar{u}_s}{\partial \bar{x}}\right)-\bar{\rho}\left(\frac{\partial \bar{u}}{\partial \bar{t}}+\bar{u}\frac{\partial \bar{u}}{\partial \bar{x}}\right)+(1-\bar{\rho})-\varepsilon(\bar{u}-\bar{u}_s)=0. \tag{10c}$$

We assume that the solution to this perturbation problem can be expanded in such a way that, for any quantity Φ,

$$\Phi(x,t)=\Phi_0+\phi\cdot\exp(kc_i t)\cdot\exp[ik(x-c_r t), \tag{11}$$

with Φ_0 the constant solution, k the real wavenumber, kc_i the ratio of the increase of perturbation amplitude, c_r the propagating velocity of perturbation, and ϕ the amplitude.

After eq. (11) is substituted into eqs. (10a)—(10c) and the terms with high order are ignored in the three resultant algebraic equations, the condition for the system having a solution is that the determinant is zero. We obtain

$$(1+m)c^2+2c\left(u_0+mu_{s0}+\frac{i}{2}\cdot\frac{m}{k}\right)+u^2+mu_{s0}^2+i\cdot\frac{mu_{s0}}{k}=0, \tag{12}$$

where

$$m=\frac{\varepsilon_0}{1-\varepsilon_0}\cdot\overline{\rho} \quad \text{and} \quad c=c_r+ic_i. \tag{13}$$

Then we can get the ratio of the increase of perturbation amplitude

$$kc_i=\frac{m^{1/2}}{1+m}\cdot\left\{-\frac{1}{2}m^{1/2}\pm\frac{1}{2^{1/2}}\left[\left(w_0^2k^2+\frac{1}{4}m\right)^2+w_0^2k^2\right]^{1/4}\left[1+\frac{w_0^2k^2+\frac{1}{4}m}{\left[\left(w_0^2k^2+\frac{1}{4}m\right)^2+w_0^2k^2\right]^{1/2}}\right]^{1/2}\right\}, \tag{14}$$

where $w_0=u_0-u_{s0}$.

The contours of kc_i on k-w_0 plane are shown in Fig. 5 (+ is taken for the sign

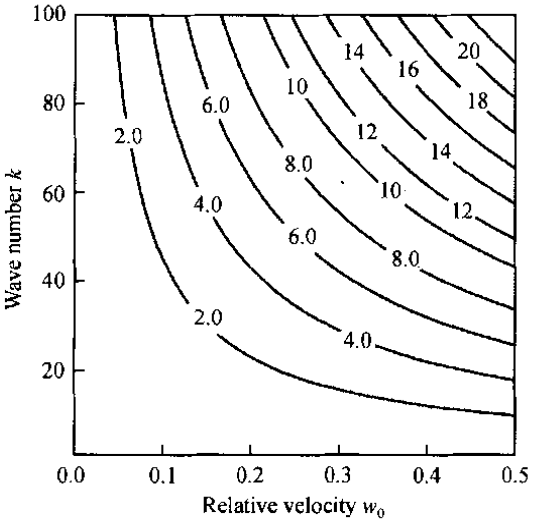

Fig. 5. Contour of kc_i on k-w_0 plane.

$\pm$ in eq. (14)). It should be noted that kc_i is always positive in the first quadrant with $k>0$ and $w_0>0$. This indicates that the sedimentation and seepage process is always unstable with such a kind of two-phase flow model.

It is obviously not coincident with the experimental results described in refs. [1] and [2], especially for the case in which the size of sand grains is uniform and no cracks or eroded pathways would be observed. Because the size distribution of sand grains and the stress in the sand skeleton are not taken into account and the initial liquefied sand is considered to be even in this model, the stability analysis with this kind of two-phase flow model cannot produce a satisfactory explanation for the development of cracks and eroded pathways in liquefied sand.

4 Transportation and erosion of fine sand grains

To give an explanation of the formation of extended horizontal cracks in a vertical sand column, Cheng et al. proposed a three-phase flow model[7]. It has been shown that unevenness in permeability along the length of the sand column is essential in causing cracks to develop. In this study we examined the transportation of the fine component of sand through an erosion/deposition process and how small initial unevenness in permeability or stratification is amplified by percolation.

As the fine sand grains may be washed away by the percolating water, the percolating water becomes turbid and the initial porosity will be altered in both time and space. An eroded fine sand slurry percolating through porous sand can be described in terms of a three-phase flow in the following manner. In addition to porosity $\varepsilon(x,t)$, we define $q(x,t)$ as the volume fraction or specific volume of sand carried in the percolating slurry and $Q(x,t)$ as the specific mass of sand lost to the percolating slurry. Then the simplified governing equations for the liquefied part of saturated sand can be written as

$$\frac{\partial(\varepsilon-q)\rho}{\partial t}+\frac{\partial(\varepsilon-q)\rho u}{\partial x}=0, \tag{15}$$

$$\frac{\partial q\rho_s}{\partial t}+\frac{\partial q\rho_s u}{\partial x}=\frac{\partial Q}{\partial t}, \tag{16}$$

$$\frac{\partial(1-\varepsilon)\rho_s}{\partial t}+\frac{\partial(1-\varepsilon)\rho_s u_s}{\partial x}=-\frac{\partial Q}{\partial t}, \tag{17}$$

$$\varepsilon\frac{\partial p}{\partial x}+\frac{\varepsilon^2}{K}(u-u_s)+[(\varepsilon-q)\rho+q\rho_s]g=0, \tag{18}$$

$$\frac{\partial p}{\partial x}+(\varepsilon-q)\rho g+(1-\varepsilon+q)\rho_s g=0. \tag{19}$$

We can further simulate the erosion/deposition process using the following empirical relations:

$$\begin{aligned}
&\frac{1}{\rho_s}\frac{\partial Q}{\partial t}=\frac{\lambda}{T}\left(\frac{u-u_s}{u^*}-q\right), \quad \text{if} \quad \frac{Q}{\rho_s}\leqslant\frac{Q_c(x)}{\rho_s},\\
&\frac{1}{\rho_s}\frac{\partial Q}{\partial t}\leqslant 0, \qquad \text{otherwise,}\\
&K=K(\varepsilon,q),
\end{aligned} \tag{20}$$

where the first term on the right side of the first equation in eq. (20) shows how sand is transferred to water. The second term describing deposition places a limit on the amount of sand that can be carried in the fluid. $Q_c(x)$ is the maximum amount of sand available that can be washed away from a unit volume element at x. For simplicity, $Q_c(x)$ is assumed to be given and to be independent of the flow rate and the state of sand. T and u^* are empirical constants. λ is a small parameter and is employed to obtain an asymptotic solution. $K(\varepsilon,q)$, the permeability, is now assumed to be a fast varying or sensitive function of q as well as ε:

$$K(\varepsilon,q)=K_0e^{-\alpha q+\beta\varepsilon}, \quad 1\ll\beta\ll\alpha. \tag{21}$$

We let $\beta\ll\alpha$ in order to make K more sensitive to q than to ε. Eqs. (15) to (20) form a closed set of equations describing the three-phase system.

Given that the assumption of incompressibility is still valid, the first three mass conservation equations (15)—(17) can then be integrated to yield

$$\varepsilon u+(1-\varepsilon)u_s=U(t), \tag{22}$$

where $U(t)$ is the flow rate of water and sand per unit cross-sectional area of the sand column, which can be determined by boundary conditions. By eliminating $\frac{\partial p}{\partial x}$ from the two momentum conservation equations (18) and (19), we obtain

$$\begin{aligned}
u_s&=u-\frac{Kg}{\varepsilon}\left[(\varepsilon-q)\rho+(1-\varepsilon+q)\rho_s-\frac{1}{\varepsilon}\left[q\rho_s+(\varepsilon-q)\rho\right]\right]\\
&=u-\frac{Kg}{\varepsilon}(1-\varepsilon)(\varepsilon-q)(\rho_s-\rho).
\end{aligned} \tag{23}$$

Then we get the velocity of water $u(\varepsilon,q)$:

$$u=U(t)+\frac{(1-\varepsilon)^2}{\varepsilon^2}Kg(\varepsilon-q)(\rho_s-\rho). \tag{24}$$

Substituting eq. (24) into eqs. (15) and (16), we obtain equations to solve $\varepsilon(x,t)$ and $q(x,t)$:

$$\frac{\partial \varepsilon}{\partial t}+\frac{\partial \varepsilon u}{\partial x}=\frac{1}{\rho_s}\frac{\partial Q}{\partial t}=\frac{\lambda}{T}\left(\frac{u-u_s}{u^*}-q\right), \tag{25}$$

$$\frac{\partial q}{\partial t}+\frac{\partial qu}{\partial x}=\frac{1}{\rho_s}\frac{\partial Q}{\partial t}=\frac{\lambda}{T}\left(\frac{u-u_s}{u^*}-q\right). \tag{26}$$

From eqs. (24)—(26) combining initial and boundary conditions, u, ε, and q can be calculated by a numerical method.

An example to use the three-phase flow model

In ref. [7], although discussion was focused on the formation of horizontal cracks, the specific volume of sand carried in the percolating fluid, $q(x,t)$, was also given under a further assumption. As the sand sits on a perforated rigid diaphragm, u_s can be set to zero. Then eqs. (15)—(20) yield

$$\varepsilon(x,t)-\varepsilon_0(x)=\frac{Q}{\rho_s}, \tag{27}$$

$$\varepsilon(x,t)u(x,t)=U(t), \tag{28}$$

$$\frac{\partial q}{\partial t}+\frac{\partial qu}{\partial x}=\frac{\partial \varepsilon}{\partial t}, \tag{29}$$

$$\frac{\partial \varepsilon}{\partial t}=\frac{\lambda}{T}\left(\frac{u}{u^*}-q\right). \tag{30}$$

The unknown quantities can be solved subject to the following initial and boundary conditions:

$$\varepsilon(x,0)=\varepsilon_0(x),\quad q(x,0)=0,\quad Q(x,0)=0,\quad \varepsilon(0,t)u(0,t)=U(t),\quad q(0,t)=0. \tag{31}$$

Carrying out the asymptotic solution, we obtain

$$u(x,t)=\frac{U(t)}{\varepsilon_0(x)}-\lambda\frac{U(t)}{Tu^*\varepsilon_0^3(x)}\int_0^t U(\tau)\mathrm{d}\tau+O(\lambda^2), \tag{32}$$

$$\varepsilon(x,t)=\varepsilon_0(x)+\lambda\frac{1}{Tu^*\varepsilon_0(x)}\int_0^t U(\tau)\mathrm{d}\tau+O(\lambda^2), \tag{33}$$

$$\frac{Q(x,t)}{\rho_s}=\lambda\frac{1}{Tu^*\varepsilon_0(x)}\int_0^t U(\tau)\mathrm{d}\tau+O(\lambda^2). \tag{34}$$

The calculation of q is somewhat complicated. The zeroth order term in q is clearly equal to zero. The first order term $q_1(x,t)$ satisfies the following equation:

$$\frac{\partial q_1}{\partial t}+\frac{U(t)}{\varepsilon_0(x)}\frac{\partial q_1}{\partial x}-q_1\frac{U(t)}{\varepsilon_0^2(x)}\frac{d\varepsilon_0(x)}{dx}=\frac{U(t)}{Tu^*\varepsilon_0(x)}, \tag{35}$$

of which the characteristics satisfy the following equation:

$$\frac{\mathrm{d}x}{\mathrm{d}t}=\frac{U(t)}{\varepsilon_0(x)}. \tag{36}$$

The characteristics relating x and t are implicitly given by

$$\begin{aligned}\int_{x_0}^{x}\varepsilon_0(\xi)\mathrm{d}\xi&=\int_0^t U(\tau)\mathrm{d}\tau,\\ \int_0^x\varepsilon_0(\xi)\mathrm{d}\xi&=\int_{t_0}^t U(\tau)\mathrm{d}\tau.\end{aligned} \tag{37}$$

The first set of curves based on the parameter x_0 gives characteristics originating from the x axis. The second set of curves based on the parameter t_0 gives those originating from the time axis. Integrating along a characteristic originating from the x axis, $x=x(x_0,\ t)$ and x_0 between 0 and H (the height of sand column), we obtain a formal expression for $q_1(x,t)$:

$$q_1(x)=\frac{1}{Tu^*}\varepsilon_0(x)\int_{x_0}^{x}\frac{\mathrm{d}\xi}{\varepsilon(\xi)}. \tag{38}$$

To show how q varies with x and t, we assume $U(t)=U_0=\text{const}$; namely, there is a steady water flow through the diaphragm on which the sand sample sits, and

$$\varepsilon_0(\xi)=0.3(1-0.1\cos 4\pi\xi),\quad \xi=\frac{x}{H}. \tag{39}$$

$q_1(\xi)$ along characteristics can then be calculated using eq. (38) and is shown in Fig. 6 for $\xi_0=0,\ 0.1,\ \cdots,\ 0.9$. The corresponding characteristics are shown in Fig. 7. To find $q_1(\xi)$ at a given time $\frac{tU_0}{H}$, we can draw a horizontal line in Fig. 7. The intersection of this line with the $\xi_0=0$ characteristic locates a ξ (note that $\xi=\xi(\xi_0,\ 0)$). These two values together determine the value of $q_1(\xi)$ from Fig. 6. Repeating the

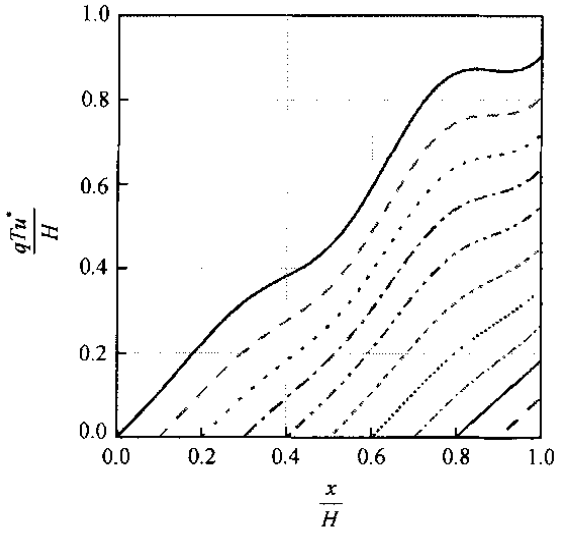

Fig. 6. q_1 along C.

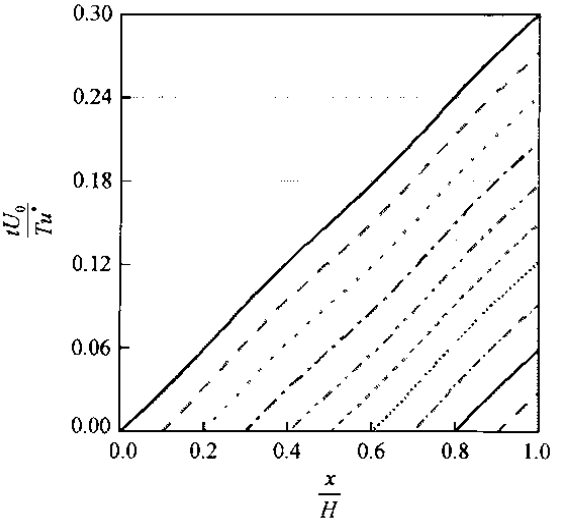

Fig. 7. Characteristics C.

same procedure for other values of ξ_0 we find all values of $q_1(\xi)$ for this particular time. To obtain $q_1(\xi)$ for smaller values of ξ, we note that all characteristics originating from the time axis are constructed by simply displacing the characteristic for $\xi_0 = 0$ along the time axis by appropriate amounts. Hence, the initial portion of the q-ξ curve for $\xi_0 = 0$ is shared by all q-ξ curves. The characteristic for $\xi_0 = 0$ reaches the top of the sand column at $t = t_m$ which in our numerical example is $\frac{t_m U_0}{H} = 0.3$. For all times greater than t_m, on the first order of approximation, $\varepsilon = \varepsilon_0(\xi)$ and the distribution

of q along x no longer changes with time. The first order perturbation in q in the dimensionless form $\frac{q_1(x)Tu^*}{H}$ at $\frac{tU_0}{H}=0.12$ is shown in Fig. 8.

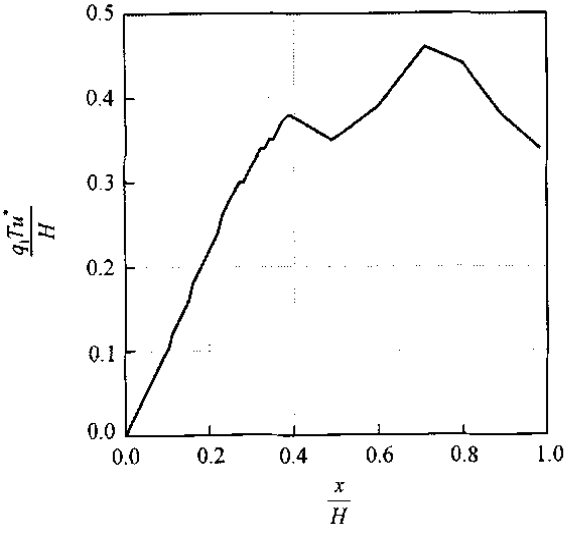

Fig. 8. q_1 at $\frac{tU_0}{H}=0.1$.

It should be noted that transport of the fine component of sand tends to increase q along x in a general way, and q is the principal cause for the decrease in permeability.

5 Remarks

Since cracks occur where the permeability is close to being the smallest, the experimentally observed inhomogeneity in permeability both spacial and temporal is a question deserving further examination. X-ray image analysis is useful to detect cracks and drainage pathways in saturated sand and is helpful to construct a new model to study the mechanism of the transportation of fine sand and the formation of cracks. The two-phase flow model employed in this paper cannot generate the expected result coincident with that observed in the experiment. A three-phase flow model was then introduced in this paper, and it proved that small initial unevenness in permeability or stratification can be amplified by percolation which transports the fine component of the sand through an erosion/deposition process. The erosion/deposition model does appear to include the main features of the transportation and accumulation of fine sand. However, to get more quantitative results, further experimental and theoretical work needs to be done.

Acknowledgements The authors wish to thank all their colleagues in the Institute of Mechanics, CAS, for their valuable discussion on various parts of the work described in the paper, particularly Associate Professor Lu Xiaobing who has provided more support. This work was supported by the National Natural Science Fundation of China (Grant No. 10372104), the Special Funds for Major State Basic Research Project (Grant No. 2002CB412706),

the National Natural Science Fundation of China (Grant No. 10372104), the Knowledge Innovation Project of Chinese Academy of Sciences (Grant No. KJCX2-SW-L1-2) and the Special Research Project for Landslide and Bank-collapse in The Three Gorges Reservoir Areas (Grant No. 4-5).

References

1. Zhang, J. F., Meng, X. Y., Yu, S. B. et al., Experimental study on permeability and settlement of saturated sand under impact load, Acta Mechanica Sinica (in Chinese), 1999, 31 (2): 230—237.
2. Peng, F. J., Tan, Q. M., Zheng, Z. M. et al., Laboratory study on cracks in saturated sands, Acta Mechanica Sinica, 2000, 16(1): 48—53.
3. Seed, H. B., Design problems in soil liquefaction, Journal of Geotechnical Engineering, ASCE, 1987, 113(8): 827—845.
4. Fiegel, G. L., Kutter, B. L., Liquefaction mechanism for layered soils, Journal of Geotechnical Engineering, ASCE, 1994, 120 (4): 737—755.
5. Kobusho, T., Water film in liquefied sand and its effect on lateral spread, J Geotechnical and Geoenvironmental Engineering, 1999, 125(5): 817—826.
6. Prosperitti, A., Satrape, J. V., Stability of two-phase flow models, Two Phase Flows and Waves, The IMA Volumes in Mathematics and Its Applications, Vol. 26 (eds. Joseph, D. D., Schaeffer, D. G.), New York: Springer-Verlag, 1990, 98—117.
7. Cheng, C. M., Tan, Q. M., On the mechanism of the formation of horizontal cracks in a vertical column of saturated sand, Acta Mechanica Sinica, 2001, 17(1): 1—9.
8. Baxter, G. W., Behringer, R. P., Fagert, T. et al., Pattern formation and time-dependence in flowing sand, Two Phase Flows and Waves, The IMA Volumes in Mathematics and Its Applications, Vol. 26 (eds. Joseph, D. D., Schaeffer, D. G.), New York: Springer-Verlag, 1990, 1—29.